BiVO$_4$ nanowires decorated with CdS nanoparticles as Z-scheme photocatalyst with enhanced H$_2$ generation

Fan Qi Zhou [a], Jin Chen Fan [a,*], Qun Jie Xu [a,*], Yu Lin Min [a,b,*]

[a] Shanghai Key Laboratory of Materials Protection and Advanced Materials in Electric Power, College of Environmental and Chemical Engineering, Shanghai University of Electric Power, 200090, China
[b] Shanghai Key Lab of Chemical Assessment and Sustainability, China

ABSTRACT

Highly efficient photocatalysts require to be achieved *via* an efficient charge separation action and responded under visible light. Here, we demonstrate a novel Z-scheme heterojunction photocatalyst composed of two visible light responding semiconductors without use of electron mediator. The as-prepared CdS nanoparticles decorated BiVO$_4$ nanowires (CdS/BiVO$_4$ NWs) exhibit broader light absorption region and Z-scheme charge separation mechanism for photocatalytic H$_2$ generation under visible light. As a results, the optimizing CdS/BiVO$_4$ NWs in 1:2 wt ratio shows more than two times increase in photocatalytic H$_2$ generation rate compared to bare CdS. Moreover, the Z-scheme CdS/BiVO$_4$ NWs lead to main oxidation sites at BiVO$_4$ NWs that successfully avoid photo-corrosion of CdS during photocatalysis.

© 2016 Published by Elsevier B.V.

1. Introduction

Energy crisis and global warming caused by fossil fuel combustion have attached a lot attention [1,2]. Photocatalysis as green and clean approach is regarded as one of the most intriguing ways to solve these problems [3–7]. Superior to solo photocatalysts, the Z-scheme system is comprised of more than two semiconductors that could promote the spatial separation of charge carrier and separate reduction and oxidation reaction at two sides [8,9]. In the view of water-splitting system, the photogenerated electrons in the higher conduction band (CB) could take part in H$_2$ evolution and labeled as photosystem II (PS II), while holes in the lower valence band (VB) could take part in O$_2$ evolution and labeled as photosystem I (PS I).

In aforementioned two components in Z-scheme system, cadmium sulfide (CdS) is one of most promising PS II candidate because of the suitable band gap (2.25 eV) and ideal CB position for the H$_2$ generation and light harvesting. For instance, the Z-scheme systems of TiO$_2$/Au/CdS [9–11], TiO$_{1.96}$C$_{0.04}$/Au/CdS [12], TiO$_2$/Ag/CdS [13], and ZnO/Au/CdS [14] have demonstrated highly efficient solar energy conversion. Unfortunately, in addition to noble metal use as electron shuttle media in these Z-scheme systems, the PS I photo-catalysts were mainly TiO$_2$ and ZnO, which led to its photoactivity only under UV light, limiting its practical application in visible region. So it is attractive to construct a Z-scheme, which consists of two photocatalysts without redox mediators but with visible light response ability. On the basis of above two factors, lowering CB position of PS I photocatalyst to be close to VB position of CdS seems to be responsible for noble metal use as well as enhancing visible harvesting. On this point, Zhang et. al and Jin et. al took advantage of WO$_3$ as PS I photocatalyst substitute for TiO$_2$ or ZnO without using noble metal as redox mediators [15,16]. In addition to WO$_3$, BiVO$_4$ has been widely employed as PS I photocatalyst in Z-scheme system, which owns not only a narrower bandgap (2.4 eV) to harvest more solar light [17,18], but also a similar CB position as WO$_3$. In previous studies, the BiVO$_4$ photocatalyst was combined with Ru-SrTiO$_3$: Rh [19,20] or Zn$_x$Cd$_{1−x}$Se [21], by which the charge separation could be remarkably improved for solar water splitting. Owing to suitable bandgaps and band potentials between CdS and BiVO$_4$, it is expected that photogenerated electrons on CB of BiVO$_4$ could rapidly recombine with photogenerated holes on VB of CdS to realize a novel Z-scheme system, moreover, both CdS and BiVO$_4$ could absorb light expanding to high wavelength due to their narrow bandgaps. We note that the CdS/BiVO$_4$ hybrid is beneficial to the separation of photogenerated charges [22,23]. We are also aware that the CdS/BiVO$_4$ hybrid has been studied in photoelectro-chemical water splitting and selective reduction of nitroaromatic compounds. However, reports on photocatalytic H$_2$ generation and

degradation of dye using hierarchical CdS/BiVO$_4$ hybrid have not been indicated.

Inspired by the progress in 1D nanostructures for solar energy conversion, and the reduction sites located on CdS surface, we have designed hierarchical CdS/BiVO$_4$ hybrid composed of CdS nanoparticles decorated on 1D BiVO$_4$ nanowires to form Z-scheme heterostructures. Photocatalytic H$_2$ evolution has been studied under visible light irradiation by using lactic acid as hole scavenger. And a target Rh.B dyes have been chosen as model to investigate its photocatalytic activity compared with individual CdS and BiVO$_4$ under visible light.

2. Experimental section

2.1. Synthesis of 1D CdS/BiVO$_4$ nanowires

All of the reagents were analytical grade and used without further purification. The BiVO$_4$ nanowire synthesis was based on the procedure reported previously [19]. 1 mmol V$_2$O$_5$ power and 2 mmol of Na$_2$SO$_4$ were dissolved into 40 mL of deionized water with stirring. The mixture was then transferred to a 50 mL Teflon-lined autoclave at 180 °C for 24 h. The obtained Na$_2$V$_6$O$_{16}$·3H$_2$O nanowire and Bi(NO$_3$)$_3$·5H$_2$O with 1:6 molar ratio was dispersed into 40 mL ethanol-water solution in 4:1 vol ratio, which was then heated in a 50 mL Teflon-lined autoclave at 120 °C for 24 h to obtain BiVO$_4$ nanowires. The BiVO$_4$ nanowires were filtered and washed several times with deionized water and absolute ethanol and dried at 50 °C for 10 h. The CdS nanoparticles were synthesized by mixing 0.01 mol Na$_2$S·9H$_2$O and 0.01 mol Cd(Ac)$_2$·2H$_2$O in 40 mL water. The resulted CdS nanoparticles were centrifuged and washed with deionized water, and dried at 50 °C under a vacuum condition. The 1D CdS/BiVO$_4$ nanowires were synthesized by ultrasonically dispersing different weight ratios of CdS nanoparticles and 1D BiVO$_4$ nanowires into 40 mL ethylene glycol and heated at 200 °C for 72 h in 50 mL Teflon-lined autoclave. The yellow precipitates were collected and washed with deionized water and absolute ethanol, then dried at 50 °C under a vacuum condition. The weight ratios between CdS and BiVO$_4$ were controlled to be 1:1, 1:2, 1:5 and 1:10 respectively.

2.2. Characteristics of 1D CdS/BiVO$_4$ nanowires

XRD patterns were performed with a diffractometer on Rigaku, Japan, RINT 2500 V using Cu Kα radiation. Diffuse reflectance UV–vis absorption spectra were recorded using a spectrophotometer (Shimadzu UV-2401PC) equipped with a diffuse reflectance accessory, and BaSO$_4$ was used as the reference. Transmission electron microscopy (TEM) observations were obtained using a JEM-2200FS microscope with Cs correction. Scanning electron microscopy (SEM) images were taken on a field emission scanning electron microscope (FESEM, JEOL, FEG-XL 30S). XPS analysis was performed with an ESCALAB-220I-XL (THERMO-ELECTRON, VG Company) device. Photoluminescence was recorded at room temperature using a fluorescence spectrometer (Shimadzu, RF-5410PC). Photocurrent measurements were performed in a homemade three electrode system. The working electrode was prepared *via* sample containing slurry on ITO with area of 1.05×1.05 cm^{-2}. Measurements of the photocurrent collected were carried out with a potentiostat (CHI660C).

2.3. Photocatalytic test

2 wt.% Pt was photo-deposited in mixed H$_2$PtCl$_6$ and lactic acid electrolyte under solar light irradiation, the resulted samples was washed with water several times and dried in oven at 60 °C. Photocatalytic hydrogen evolution was carried out in a Pyrex top-irradiation reaction vessel connected to a closed glass gas system. In detail, 50 mg of photocatalyst was dispersed in the 200 mL lactic acid (20 vol.%) solution or 1 M Na$_2$SO$_3$ solution and irradiated under 300 W Xe lamp with 420 nm cutting off. The H$_2$ amounts was analyzed using a gas chromatograph equipped with a thermal conductivity detector (TCD).

For photodegradation of organic dyes, the decomposition reaction of a 50 mL Rh.B (2×10^{-5} M) aqueous solution was carried out. A powdered sample of 30 mg was dispersed in the Rh.B solution under ultrasonication for 1 min, and then was kept in dark conditions for 1.5 h. For the irradiation system, a 300 W Xe lamp with 420 nm filter was used at the distance of 100 mm from the solution in a darkness box. The suspension was irradiated for different irradiation times. The samples were then withdrawn regularly from the reactor and the dispersed powder was removed through centrifugation. The clean transparent solution was analyzed by UV–vis spectroscopy. The concentration of Rh.B in the solution was determined as a function of irradiation time from the absorbance region at a functional wavelength.

3. Results and discussion

Fig. 1a shows the XRD patterns of the CdS nanoparticle, BiVO$_4$ NWs and CdS/BiVO$_4$ NWs hybrids. The XRD pattern of CdS indicates the present of hexagonal phase (JCPDS no. 41–1049) while BiVO$_4$ NWs can be assigned to monoclinic phase (JCPDS no. 14–0688). The XRD patterns of the CdS/BiVO$_4$ NWs hybrids indicate the presence of hexagonal CdS and monoclinic BiVO$_4$, simultaneously. It is notable that the diffraction peaks of BiVO$_4$ NWs is gradually dominated from 1:1 CdS/BiVO$_4$ NWs to 1:10 CdS/BiVO$_4$ NWs, but both diffraction peaks corresponding to CdS and BiVO$_4$ are obviously distinguished in all of CdS/BiVO$_4$ NWs. Fig. 1b shows the SEM image of as-prepared BiVO$_4$ NWs that have length of several micron and smooth surfaces. The HR-TEM of BiVO$_4$ NWs reveals lattice spacing of 0.255 nm, corresponding to [010] oriented growth (Fig. S1). Fig. 1c demonstrates as-synthesized 1:2 CdS/BiVO$_4$ NWs, the rough surface characters indicate a uniform coating of CdS on the BiVO$_4$ NWs (Fig. 1c). The TEM and HR-TEM of bare CdS exhibit size distribution of ~25 nm with the lattice fringes of 0.358 nm, corresponding to (100) facet of CdS (Fig. S2). TEM and HR-TEM images of 1:2 CdS/BiVO$_4$ NWs in Fig. 1d and e exhibit the CdS nanoparticle uniformly decorated on the surface of BiVO$_4$ NWs. The EDX spectrum of 1:2 CdS/BiVO$_4$ NWs reveals co-existence of Bi, Cd, V, S and O elements (Fig. 1f). The results demonstrate successful synthesis of CdS/BiVO$_4$ NWs heterojunction via ex-situ method under long-term high-temperature and pressure condition. Since the BiVO$_4$ is unstable in S^{2-} anion containing solution, it is important to develop a viable method for the CdS/BiVO$_4$ heterojunction [24].

The optical properties of BiVO$_4$ NWs, CdS and various CdS/BiVO$_4$ NWs were investigated. As shown in Fig. 2, the bare BiVO$_4$ NWs has absorption edge at 505 nm, while the absorption edge of bare CdS is located at 545 nm, both have photonic absorption ability in visible region. The absorption edges of CdS/BiVO$_4$ NWs are gradually expanded towards high wavelength with increasing CdS amount, indicating that there is optical property enhancement *via* hybridized with CdS compared to bare BiVO$_4$ NWs. The chemical interaction of CdS/BiVO$_4$ NWs was confirmed by XPS, as presented in Fig. S3. Fig. S3a clearly indicated the Cd, S, Bi, O and V as major elements in the CdS/BiVO$_4$ NWs. In comparison of Bi 4f spectra (Fig. S3b), 0.2 eV shifts toward higher binding energy with small intensity decreases can be observed from the CdS/BiVO$_4$ NWs, suggesting that the binding energy of the core level electrons of Bi in BiVO$_4$ is influenced when the CdS was introduced. For charge-balance in CdS/BiVO$_4$ NWs, the peaks of the Cd 3d also was accordingly shifted
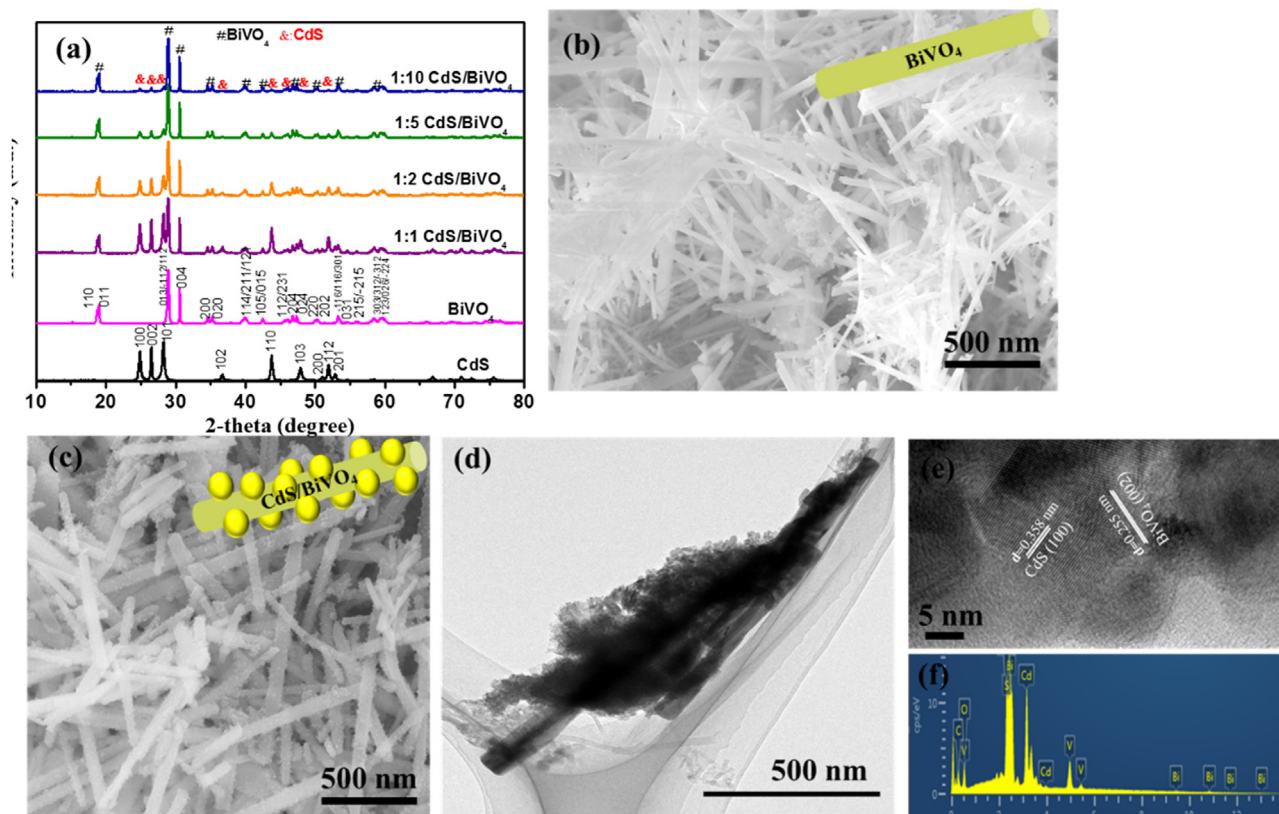
Fig. 1. (a) XRD patterns of BiVO$_4$ NWs, CdS and various CdS/BiVO$_4$ NWs. (b) SEM image of as-prepared BiVO$_4$ NWs. (c) SEM image of 1:2 CdS/BiVO$_4$ NWs. (d and e) TEM and HR-TEM image of 1:2 CdS/BiVO$_4$ NWs. (f) EDX spectrum of 1:2 CdS/BiVO$_4$ NWs.

to low binding energy by 0.7 eV compared to pure CdS (Fig. S3c). The results indicated that there is strongly chemical interaction between CdS and BiVO$_4$, rather than simple physical mixture. The BET surface areas of BiVO$_4$ NWs, CdS and 1:2 CdS/BiVO$_4$ NWs were investigated using nitrogen adsorption–desorption isotherms. As shown in Fig. 3, it could be clearly observed that three samples are type IV (Brunauer–Deming–Deming–Teller (BDDT) classification) due to the presence of mesopores [25,26]. The special surface areas of BiVO$_4$ NWs, CdS and 1:2 CdS/BiVO$_4$ NWs are 38.6, 46.8 and 39.4 m^2/g, respectively, suggesting that the CdS decorated BiVO$_4$ NWs doesn't have a conspicuous influence on their surface area.

The photocatalytic H$_2$ generations are first performed in lactic acid electrolyte under visible light irradiation (>420 nm, UV-cutoff filter) and 2 wt.% Pt as co-catalyst was per-deposited on all testing samples *via* photo-deposition method. Fig. 4a shows the photocatalytic H$_2$ actives over BiVO$_4$ NWs, CdS and various CdS/BiVO$_4$ NWs with/without Pt loading. The BiVO$_4$ NWs, even loaded with Pt alone are inactive for H$_2$ production, probably, because its CB position is lower than H$_2$/H$_2$O potential. The bare CdS exhibits a poor photocatalytic H$_2$ rate of 34 μmol/h, while the Pt/CdS has a photocatalytic H$_2$ rate of 568 μmol/h. The improvement of photocatalytic H$_2$ activity by order of magnitudes could be ascribed to
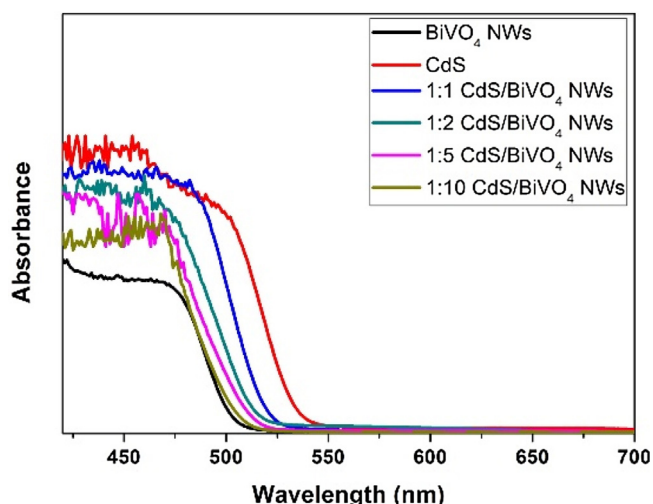

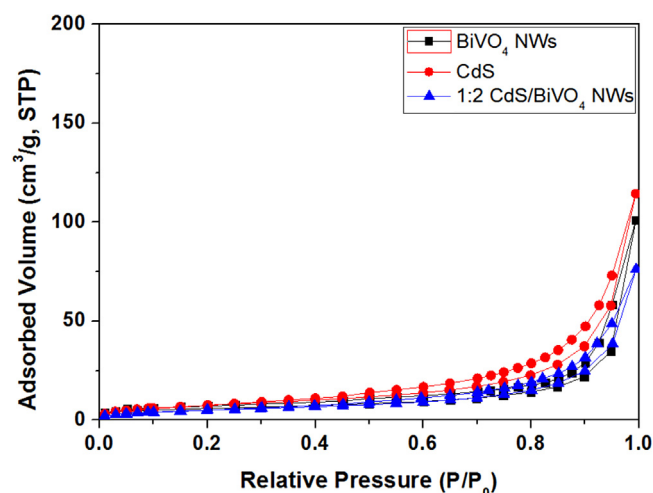**Fig. 2.** UV–vis absorption spectra of BiVO$_4$ NWs, CdS, and various CdS/BiVO$_4$ NWs.

Fig. 3. Nitrogen adsorption–desorption isotherms of BiVO$_4$ NWs, CdS, and 1:2 CdS/BiVO$_4$ NWs.
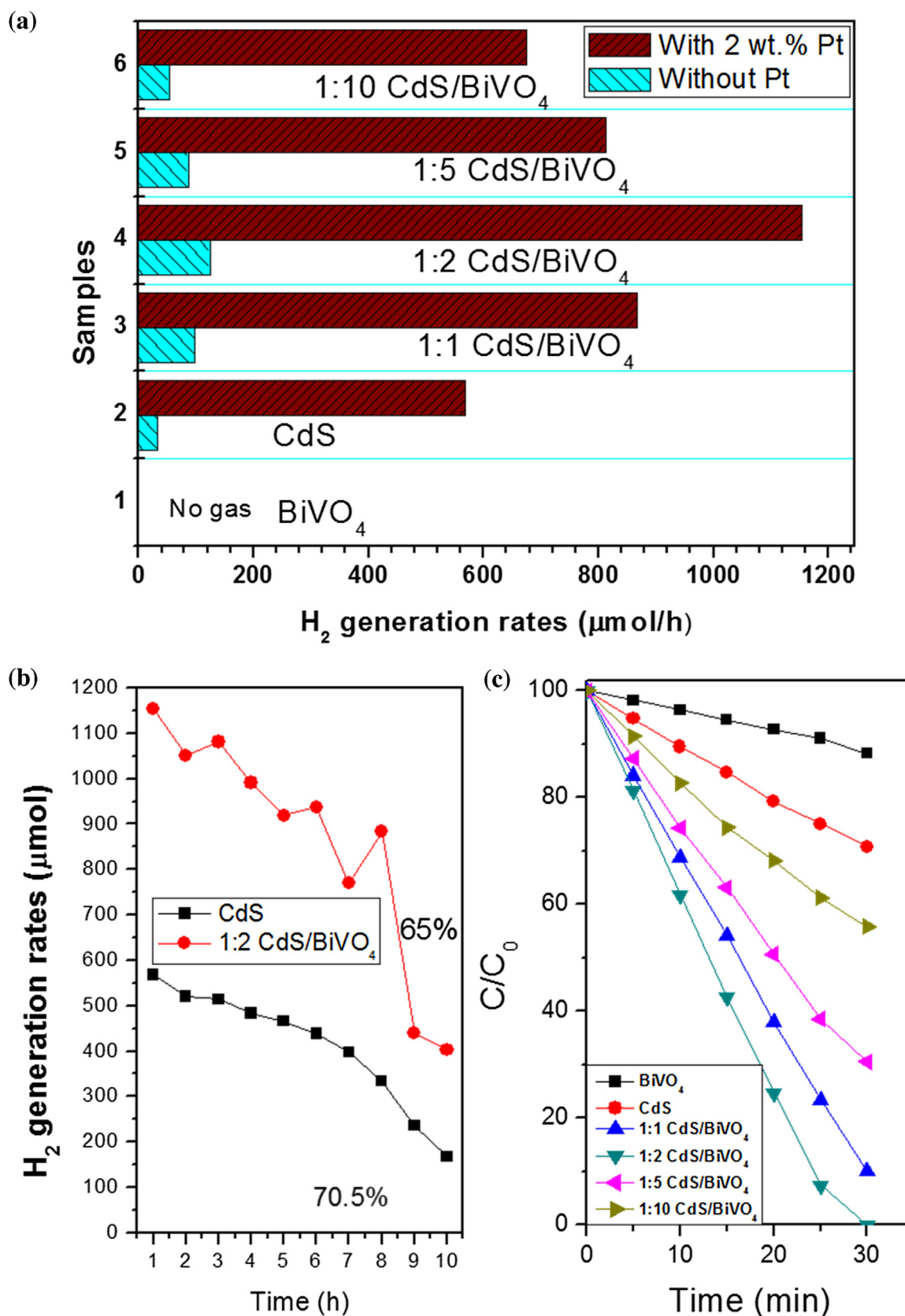
Fig. 4. (a) Photocatalytic H_2 generation rates over $BiVO_4$ NWs, CdS, and various CdS/$BiVO_4$ NWs with/without 2 wt.% Pt under visible light irradiation in lactic acid solution. (b) Photocatalytic H_2 performances fading of CdS and 1:2 CdS/BiVO4 for visible light irradiation of 10 h. (c) Photocatalytic Rh.B degradation over $BiVO_4$ NWs, CdS, and various CdS/$BiVO_4$ NWs under visible light irradiation.
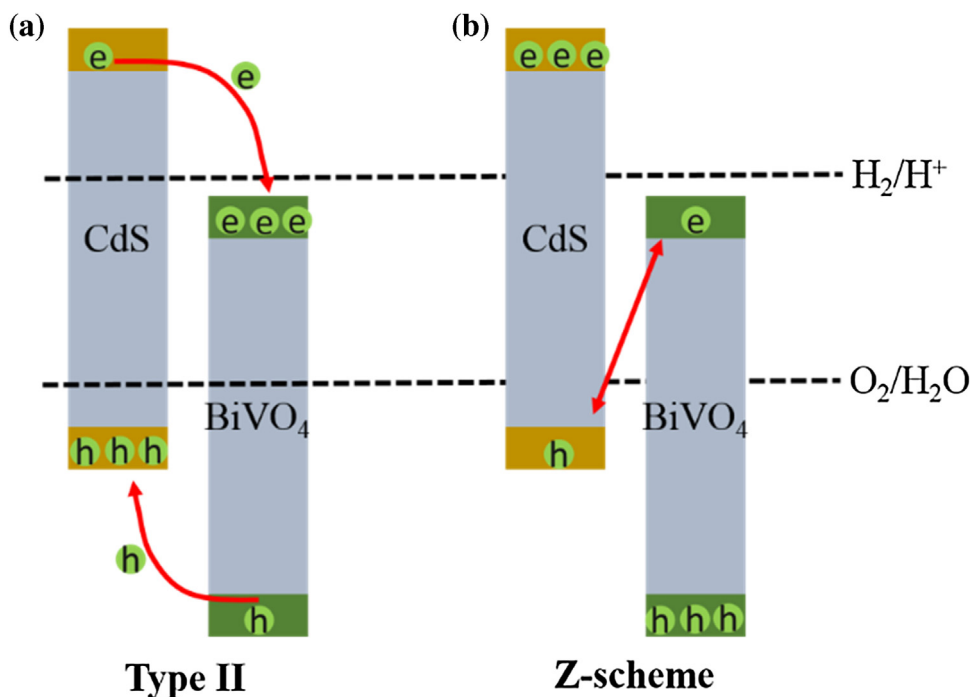
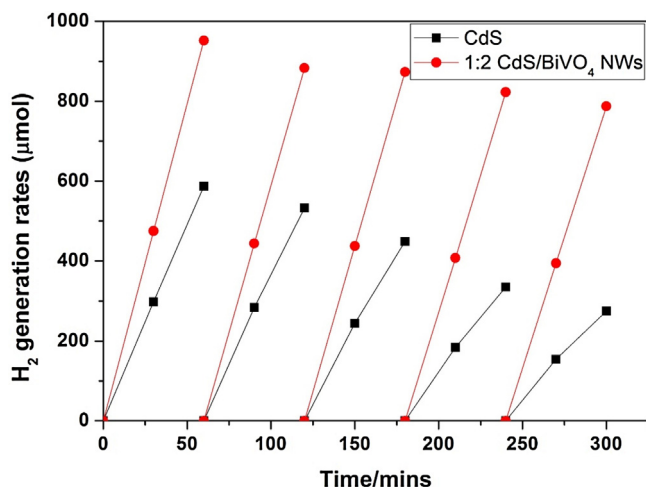**Fig. 5.** Possible charge separation diagrams of CdS/BiVO$_4$ NWs.

Fig. 6. Photocatalytic H$_2$ generation rates over 2 wt.% Pt loaded CdS and 1:2 CdS/BiVO$_4$ NWs under visible light irradiation in 1 M Na$_2$SO$_3$ solution.

bifunctions of Pt during photocatalysis, one promotes charge separation, and another enhances H$_2$ evolution. The photocatalytic H$_2$ rates of 1:1, 1:2, 1:5, 1:10 CdS/BiVO$_4$ NWs without Pt loading are 98, 124, 86 and 53 µmol/h, respectively, which are further increased to 867, 1153, 812, and 675 µmol/h after loaded with Pt, respectively. At optimized condition, 1:2 CdS/BiVO$_4$ NWs, the photocatalytic H$_2$ rates could be significantly improved by 3.65 times without Pt loading, and by 2.03 times with Pt loading compared to bare CdS. It is well-known that CdS nanoparticles alone have unsatisfied separation efficiency of photo-induced charges and poor catalytic activity for H$_2$ evolution. Therefore, we hypothesize that the enhanced photocatalytic H$_2$ activity is ascribed to charge separation at CdS and BiVO$_4$ NWs interface. By mean of Pt photodeposition, the electron accumulation at either CdS or BiVO$_4$ would be active for Pt deposition. As well-known, Pt is most promising co-catalyst for H$_2$ evolution because of the zero-approaching overpotential and excellent electron acceptor. The electron accumulated at either CdS or

BiVO$_4$ would favor electron transfer to Pt, hence efficiently accelerating H$_2$ evolution. However, the hole scavenger selectivity was limited to lactic acid because BiVO$_4$ is unstable in commonly used Na$_2$S electrolyte [24]. The lactic acid oxidation will lead to poisoning phenomenon of Pt by the —CO group from the degradation of lactic acid [27], resulting in poor stability. As shown in Fig. 4b, the 1:2 CdS/BiVO$_4$ and CdS loaded with Pt shows 65% and 70.5% of performance fading after 10 h irradiation, respectively. It is therefore expected that the stability of CdS/BiVO$_4$ is able to be improved if other kinds of co-catalyst with anti-poisoning are employed, such as MoS$_2$, WS2, WC et al. [28–33]. Photocatalytic activity of the BiVO$_4$ NWs, CdS and various CdS/BiVO$_4$ NWs were further investigated, photodegradation of Rh.B as target photocatalysis was carried out under visible light. As displayed in Fig. 4c, complete photodegradation of Rh.B only took 35 min for the 1:2 CdS/BiVO$_4$, while only about 11.7% and 29.1% of RhB molecules can be decomposed for the BiVO$_4$ NWs and CdS, respectively. And the order of photocatalytic actives for Rh.B degradation over different CdS/BiVO$_4$ is consistent with their photocatalytic H$_2$ activities.

In general, the charge separation mechanism in heterojunction with different band gaps and edge positions has several types [34]. Considering the band gap levels of CdS and BiVO$_4$ that the charge separation could be estimated to be type II or Z-scheme, as shown in Fig. 5. In type II, the photo-induced electron/hole pairs by CdS and BiVO$_4$ are separated to opposite direction, which means the electrons will be finally accumulated on CB of BiVO$_4$, while holes on VB of CdS. On the contrary, the electron/hole pairs separation by Z-scheme will result in leaving electrons on CB of BiVO$_4$ and holes on VB of BiVO$_4$. To determine the possible mechanism, the photocatalytic H$_2$ generations over Pt/CdS and 1:2 CdS/BiVO$_4$ NWs are further performed in 1 M Na$_2$SO$_3$ electrolyte. It is well-known that the CdS has seriously photo-corrosion via S^{2-} oxidation, which usually needs to be inhibited in presence of mixed Na$_2$SO$_3$ and Na$_2$S sacrificial agent [35–37]. Therefore, it is expected that there is photo-corrosion occurrence in absence of Na$_2$S electrolyte when the oxidation sites locate at VB of CdS that would discount photocatalytic H$_2$ generation stability. As shown in Fig. 6, bare CdS shows rapid decrease of photocatalytic H$_2$ activity that is almost
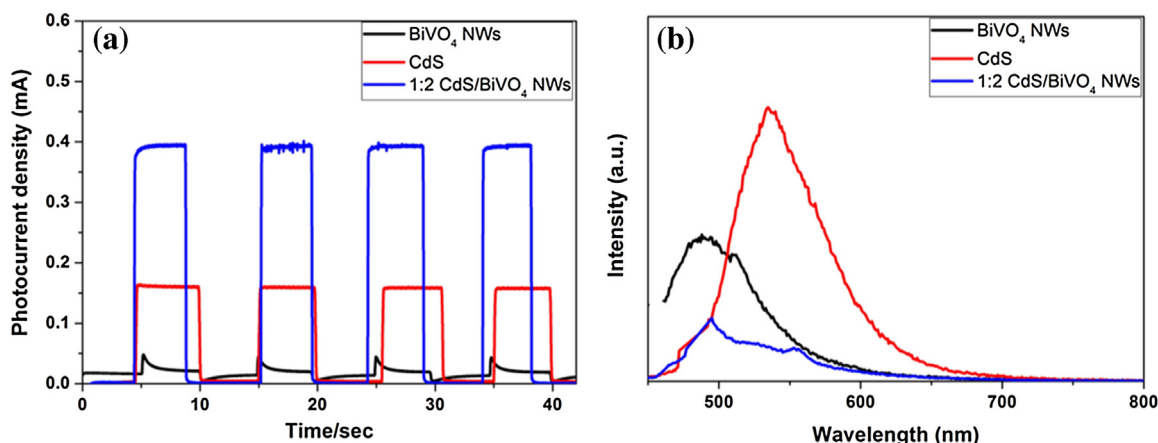
Fig. 7. (a) Transient photocurrent responses of BiVO$_4$ NWs, CdS and 1:2 CdS/BiVO$_4$ NWs under visible light irradiation in 1 M Na$_2$SO$_4$ solution at 0.1 V bias vs. Ag@AgCl. (b) Photoluminescence (PL) spectra of BiVO$_4$ NWs, CdS and 1:2 CdS/BiVO$_4$ NWs excited by 360 nm.
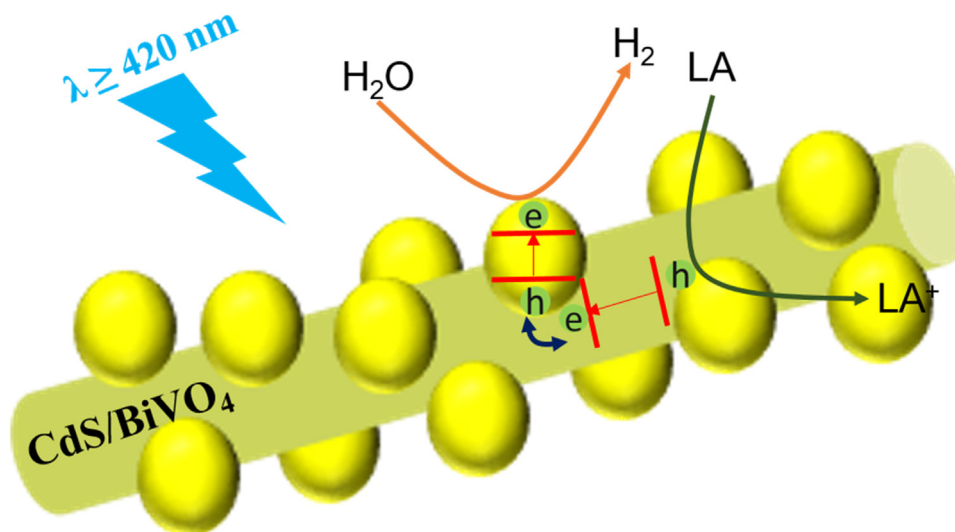

Fig. 8. Schematic illustration of the proposed Z-scheme mechanism toward photocatalytic H2 generation over CdS/BiVO4 NWs under visible light.

53% fading of photocatalytic H$_2$ generation rate during 5 h irradiation, while the 1:2 CdS/BiVO$_4$ NWs only Exhibits 17% fading of photocatalytic H$_2$ generation. The results demonstrate that the oxidation sites are mainly located at BiVO$_4$ NWs in CdS/BiVO$_4$ NWs hybrids, corresponding to Z-scheme charge separation mechanism.

The transient photocurrent responses of BiVO$_4$ NWs, CdS and 1:2 CdS/BiVO$_4$ NWs were investigated to support the enhanced charge separation in 1 M Na$_2$SO$_4$ electrolyte at 0.1 V bias vs. Ag@AgCl. As shown in Fig. 7a, the BiVO$_4$ NWs have weak photocurrent density due to its high flat potential [38], while the CdS reveals sensitive photocurrent response with switch on/off. It is obvious that the 1:2 CdS/BiVO$_4$ NWs represent much higher photocurrent density compared to BiVO$_4$ NWs and CdS, indicating that these photo-induced electrons could be transported to substrate, while the photo-induced holes are trapped by the electrolyte. The charge separation could be further demonstrated by photoluminescence (PL) spectra, as shown in Fig. 7b. The emission peak of BiVO$_4$ NWs at 495 nm is ascribed to the band-band PL phenomenon which is equal to their band-gap energy. Accordingly, the emission peak of 535 nm could be found in PL spectrum of CdS. Obviously, above two emission peaks in the 1:2 CdS/BiVO$_4$ NWs are strongly weakened, which is the evidence of efficient charge separation.

On the basis of above results, the Z-scheme charge separation mechanism could be proposed. As shown in Fig. 8, due to both visible light responding BiVO$_4$ NWs and CdS, the electron/hole pairs could be excited under visible light, and are respectively locate at CB and VB of BiVO$_4$ NWs and CdS. According to previous reports [39,40], the VB position of CdS is around 1.85 eV vs NHE, while the CB position of BiVO$_4$ is lower than 0.1 eV vs NHE. However, according to previous reports, the work function for BiVO$_4$ is higher than that of CdS [41,42]. In CdS/BiVO$_4$ heterojunction, electrons at CB of CdS could transfer to CB of BiVO$_4$ until their work functions are the same. Then, the formation of band bending at CdS/BiVO4 interface will lead to VB position up of CdS while CB position down of BiVO$_4$. The VB of CdS and CB of BiVO$_4$ close to each other results in electron/hole recombination via Z-scheme route upon visible light illumination. The leaving electrons on CB of CdS could be further contributed to H$_2$ evolution. As a results, the Z-scheme CdS/BiVO$_4$ NWs exhibit enhanced photocatalytic H$_2$ activity and anti-corrosion. To highlight the photocatalytic H$_2$ activities by using two visible light responding photocatalyst with Z-scheme charge separation mechanism, Table 1 lists the photocatalytic H$_2$ evolution behavior of various Z-scheme photocatalyst in recent years [9,12,14,43–46]. Among these photocatalysts, 1:2 CdS/BiVO$_4$ wires in our work exhibits a highest H$_2$ evolution rate.

Table 1
Z-scheme photocatalytic H_2 generation.

PS I	PS II	Electronmediator	Light source	H_2 production ratio	Ref.
Pt/CdS (<540 nm)	TiO_2 (<387 nm)	Au	500 W Xe lamp (300 < λ < 400)	10 nmol/h	[9]
Pt/CdS (<540 nm)	$TiO_{1.96}C_{0.04}$ (<455 nm)	Au	Xe arc lamp (>420)	433.2 μmol/h	[12]
CdS (<540 nm)	ZnO (<387 nm)	Cd	300 W Xe lamp	1.17 mmol/h	[43]
$PbBi_2Nb_{1.9}Ti_{0.1}O_9$ (<444 nm)	WO_3 (<460 nm)	W	450 W Xe arc lamp (>420)	14.8 μmol/h	[44]
CdS (<540 nm)	TiO_2 (<387 nm)	Au	750 W Xe lamp	3.2 μmol/h	[11]
CdS (<540 nm)	ZnO (<387 nm)	Au	300 W Xe lamp	60.8 μmol/h	[14]
P_2W_{17} (<675 nm)	TiO_2 (<365 nm)	Pt	250 W high pressure Hg lamp (>365)	19.6 μmol/h	[45]
Pt/CdS (<540 nm)	ZnO (<387 nm)	Non	300 W Xe lamp	750 μmol/h	[46]
Pt/CdS (<540 nm)	BiVO4 (<505 nm)	Non	300 W Xe arc lamp (>420)	1153 μmol/h	This work

4. Conclusion

In this work, we have successfully synthesized a Z-scheme heterojunction photocatalyst composed of $BiVO_4$ nanowires (NWs) and CdS nanoparticles, which showed more than two times enhancement in photocatalytic H_2 generation under visible light by using lactic acid as sacrificial agent. The Z-scheme charge separation was demonstrated through comparison experiment of photocatalytic H_2 generation in Na_2SO_3 solution, the highly stable photoactivity of CdS/$BiVO_4$ NWs have determined that there is direct recombination of electrons and holes from valence band of CdS and conduction band of $BiVO_4$ NWs. Furthermore, the transient photocurrent responses and PL spectra have demonstrated the fact that the Z-scheme CdS/$BiVO_4$ NWs promote efficient charge separation which could be main contributor for H_2 generation.

Appendix A. Supplementary data

Supplementary data associated with this article can be found, in the online version, at http://dx.doi.org/10.1016/j.apcatb.2016.08.027.

References

[1] J. Nowotny, T.N. Veziroglu, Int. J. Hydrogen Energy 36 (2011) 13218–13224.
[2] M.R. Hoffmann, S.T. Martin, W. Choi, D.W. Bahnemann, Chem. Rev. 95 (1995) 69–96.
[3] B.B. Ding, H.Y. Peng, H.S. Qian, L. Zheng, S.H. Yu, Adv. Mater. Interfaces 3 (2016) 1500649.
[4] Q. Xiang, J. Yu, M. Jaroniec, Chem. Soc. Rev. 41 (2012) 782–796.
[5] X. Chen, S. Shen, L. Guo, S.S. Mao, Chem. Rev. 110 (2010) 6503–6570.
[6] K. Zhang, L.Y. Wang, J.K. Kim, M. Ma, G. Veerappan, C.L. Lee, K.J. Kong, H.Y. Lee, J.H. Park, Energy Environ. Sci. 9 (2016) 499–503.
[7] F. Zhang, C.L. Zhang, W.N. Wang, H.P. Cong, H.S. Qian, ChemSusChem 9 (2016) 1449.
[8] P. Zhou, J.G. Yu, M. Jaroniec, All-solid-state Z-scheme photocatalytic systems, Adv. Mater. 26 (2014) 4920–4935.
[9] Y.L. Min, G.Q. He, Q.J. Xu, Y.C. Chen, J. Mater. Chem. A 2 (2014) 2578–2584.
[10] H. Zhu, B. Yang, J. Xu, Z. Fu, M. Wen, T. Guo, S. Fu, J. Zuo, S. Zhang, Appl. Catal. B: Environ. 90 (2009) 463–469.
[11] S.N. Guo, Y. Zhu, Y.Y. Yan, Y.L. Min, J.C. Fan, Q.J. Xu, Appl. Catal. B 185 (2016) 315–321.
[12] H.J. Yun, H. Lee, N.D. Kim, D.M. Lee, S. Yu, J. Yi, ACS Nano 5 (2011) 4084–4090.
[13] K.P. Xie, Q. Wu, Y.T. Wang, W.X. Guo, M.Y. Wang, L. Sun, C.J. Lin, Electrochem. Commun. 13 (2011) 1469–1472.
[14] Z.B. Yu, Y.P. Xie, G. Liu, G.Q. Lu, X.L. Ma, H.M. Cheng, J. Mater. Chem. A 1 (2013) 2773–2776.
[15] L.J. Zhang, S. Li, B.K. Liu, D.J. Wang, T.F. Xie, ACS Catal. 4 (2014) 3724–3729.
[16] J. Jin, J.G. Yu, D.P. Guo, C. Cui, W.K. Ho, Small 11 (2015) 5262–5271.
[17] S.Y. Dong, J.L. Feng, Y.K. Li, L.M. Hu, M.L. Liu, Y.F. Wang, Y.Q. Pi, J.Y. Sun, J.H. Sun, Appl. Catal. B: Environ. 152–153 (2014) 413–424.
[18] S.Y. Dong, Y.R. Cui, Y.F. Wang, Y.K. Li, L.M. Hu, J.Y. Sun, J.H. Sun, Chem. Eng. J. 249 (2014) 102–110.
[19] B. Liu, C.H. Wu, J.W. Miao, P.D. Yang, ACS Nano 8 (2014) 11739–11744.
[20] A. Iwase, Y.H. Ng, Y. Ishiguro, A. Kudo, R. Amal, J. Am. Chem. Soc. 133 (2011) 11054–11057.
[21] H.S. Park, H.C. Lee, K.C. Leonard, G.J. Liu, A.J. Bard, ChemPhysChem 14 (2013) 2277–2287.
[22] B. Han, S.Q. Liu, Y.J. Xu, Z.R. Tang, RSC Adv. 5 (2015) 16476–16483.
[23] J.G. Jiang, M. Wang, R. Li, L.J. Ma, L.J. Guo, Int. J. Hydrogen Energy 38 (2013) 13069–13076.
[24] X.H. Gao, H.B. Wu, L.X. Zheng, Y.J. Zhong, Y. Hu, X.W. Lou, Angew. Chem. Int. Ed. 53 (2014) 5917–5921.
[25] R. Venu, T.S. Ramulu, S. Anandakumar, V.S. Rani, C.G. Kim, Colloids Surf. A. 384 (2011) 733–738.
[26] K.S.W. Sing, D.H. Everett, R.A.W. Haul, L. Moscou, R.A. Pierotti, J. Rouquerol, T. Siemieniewska, Pure Appl. Chem. 57 (1985) 603–619.
[27] K. Chang, Z.W. Mei, T. Wang, Q. Kang, S.X. Ouyang, J.H. Ye, ACS Nano 8 (2014) 7078–7087.
[28] K. Zhang, J.K. Kim, M. Ma, S.Y. Yim, C.L. Lee, H.J. Shin, J.H. Park, Adv. Funct. Mater. 26 (2016) 4527–4534.
[29] K. Chang, X. Hai, J.H. Ye, Adv. Energy Mater. 6 (2016) 1502555.
[30] Y.J. Yuan, D.Q. Chen, Y.W. Huang, Z.T. Yu, J.S. Zhong, T.T. Chen, W.G. Tu, Z.J. Guan, D.P. Cao, Z.G. Zou, ChemSusChem 9 (2016) 1003–1009.
[31] X. Zong, J.F. Han, G.J. Ma, H.J. Yan, G.P. Wu, C. Li, J. Phys. Chem. C 115 (2011) 12202–12208.
[32] Y.X. Pan, T.H. Zhou, J.Y. Han, J.D. Hong, Y.B. Wang, W. Zhang, R. Xu, Catal. Sci. Technol. 6 (2016) 2206–2213.
[33] Z.J. Sun, H.F. Zheng, J.S. Li, P.W. Du, Energy Environ. Sci. 8 (2015) 2668–2676.
[34] S. Choudhary, S. Upadhyay, P. Kumar, N. Singh, V.R. Satsangi, R. Shrivastav, S. Dass, Int. J. Hydrogen Energy 37 (2012) 18713–18730.
[35] K. Zhang, W.J. Kim, M. Ma, X.J. Shi, J.H. Park, J. Mater. Chem. A 3 (2015) 4803–4810.
[36] H. Park, W. Choi, M.R. Hoffmann, J. Mater. Chem. 18 (2008) 2379–2385.
[37] Q. Li, X. Li, S. Wageh, A.A. Al-Ghamdi, J.G. Yu, Adv. Energy Mater. 5 (2015) 1500010.
[38] D.K. Zhong, S.J. Choi, D.R. Gamelin, J. Am. Chem. Soc. 133 (2011) 18370–18377.
[39] D. Robert, Catal. Today 122 (2007) 20–26.
[40] Y.S. Park, K.J. McDonald, K.S. Choi, Chem. Soc. Rev. 42 (2013) 2321–2337.
[41] K. Zhang, X.J. Shi, J.K. Kim, J.H. Park, Phys. Chem. Chem. Phys. 14 (2012) 11119–11124.
[42] L. Brillson, Phys. Rev. B 18 (1978) 2431–2446.
[43] X. Wang, G. Liu, L. Wang, Z. Chen, G.Q. Lu, H.M. Cheng, Adv. Energy Mater. 2 (2012) 42–46.
[44] H.G. Kim, E.D. Jeong, P.H. Borse, S. Jeon, K. Yong, J.S. Lee, W. Li, S.H. Oh, Appl. Phys. Lett. 89 (2006) 64101–64103.
[45] N. Fu, Z. Jin, Y. Wu, G. Lu, D. Li, J. Phys. Chem. C 115 (2011) 8586–8593.
[46] X.W. Wang, G. Liu, Z.G. Chen, F. Li, L.Z. Wang, G.Q. Lu, H.M. Cheng, Chem. Commun. (2009) 3452.